JOURNAL OF PROPULSION AND POWER
Vol. 18, No. 3, May–June 2002

Development of High-Performance Airfoils for Axial Flow Compressors Using Evolutionary Computation

Ernesto Benini* and Andrea Toffolo†
University of Padova, 35131 Padova, Italy

An original multiobjective optimization method is used to support the generation of a new family of profiles for two-dimensional cascades suitable for subsonic compressors. The aim of the optimization is to maximize the pressure ratio and to minimize the profile losses of a cascade, while conforming to a functional constraint on the operating range. The method uses an evolutionary algorithm featuring a novel evaluation technique conceived for multiobjective problems and a blade-to-blade inviscid/viscous solver for calculating flow quantities. As an example, an excerpt of optimized profiles is presented, and their performances are compared with those of conventional NACA 65 profiles. The new profiles show superior design performances both in efficiency and pressure rise, as well as a tolerance to incidence angles comparable to conventional profiles. The reasons of this improvement are discussed in detail on the basis of rigorous loss analysis.

Nomenclature

b	=	streamtube thickness, m
C_l	=	lift coefficient
$C_{n,i}$	=	ith coefficient of Bezier curves
C_p	=	pressure coefficient
$\boldsymbol{F}$	=	vector of objective functions
f	=	objective function
l	=	chord length, m
M	=	Mach number
$\dot{m}$	=	mass flow rate, kg/s
p	=	pressure, Pa
p_{mut}	=	mutation probability
r	=	radius, m
Re	=	Reynolds number
T	=	pitch, m
t	=	nondimensional parameter
u	=	axial velocity, m/s
V	=	speed, m/s
v	=	tangential velocity, m/s
$\boldsymbol{x}$	=	vector of decision variables
α	=	angle of attack, $\beta_1 - \gamma_c$, deg
α_1	=	incidence angle, deg
β	=	flow angle, deg
γ	=	isentropic coefficient of gas
γ_c	=	stagger angle, deg
δ^*	=	displacement thickness, m
Θ	=	momentum thickness, m
θ	=	peripheral coordinate, deg
θ_{inl}	=	inlet metal angle, deg
θ_{out}	=	outlet metal angle, deg
ρ	=	density, kg/m^3
σ	=	solidity
ω	=	total pressure loss coefficient

Subscripts

e	=	exit
max	=	maximum
min	=	minimum
ps	=	pressure side
ss	=	suction side
te	=	trailing edge
0	=	total
1	=	upstream of the cascade
2	=	downstream of the cascade

Superscripts

is	=	isentropic
$*$	=	design value

Introduction

IN the past two decades, significant improvements in the field of gas-turbine engines have occurred following the requirements for both increased efficiency and higher aerodynamic loading of compressors. The first milestone consisted in the development of a family of nonconventional airfoils, controlled diffusion airfoils (CDA),[1] which have immediately pushed the performances of compressors to a significant higher level in comparison to standard airfoils used before. To achieve this goal, the combination of compressible potential flow codes with boundary-layer codes was straightforward to control the growth of boundary layer and the prevention of its separation.

Further advances in compressor technology were gained with the second generation of CDA for multistage bladings,[2] CDA-II. This family of airfoils followed the extension of the results for the first generation of CDA into the endwall regions. The design model combined a two-dimensional, potential blade element solution with a compressible boundary-layer calculation from hub to shroud. A vortex model including wall friction, tip clearance, and shroud cavity effects was superimposed on this base. The test performed in the mid-1980s revealed that the CDA-II had produced a 1.5% increase in efficiency and 8% higher surge margin relative to the CDA baseline. This result led to a substantial improvement in surge-free operating capability and ultimately to a greater pressure ratio available per single stage.

Such improvements showed that profile families with constrained camber and thickness distribution were no longer necessary: these could be specified almost arbitrarily by the designer to achieve the best compressor performances.

More recently, the availability of increasingly larger and faster computers has greatly encouraged the use of computational fluid dynamics (CFD), along with optimization techniques to gain further

Received 10 September 2001; revision received 21 November 2001; accepted for publication 28 November 2001.

*Researcher, Department of Mechanical Engineering; benini@dim.unipd.it. Member AIAA.

†Ph.D. Candidate, Department of Mechanical Engineering; toffolo@dim.unipd.it.

improvements in compressor performance by exploring nonconventional blade configurations. Today such applications are numerous and have become popular worldwide. Obayashi[3] faced the multiobjective optimization problem of maximizing the pressure rise and efficiency of compressor cascades with a Pareto genetic algorithm and a Navier–Stokes solver. Pierret[4] used an artificial neural network coupled with a Navier–Stokes solver to maximize the efficiency and/or operating range of two-dimensional compressor cascades and then staggered them in the radial direction to obtain the three-dimensional blade. Köller et al.[5] and Küsters et al.[6] recently developed a new family of compressor airfoils, characterized by low total pressure losses and larger operating range with respect to standard CDA, using a gradient optimization method and an inviscid/viscous code.

The use of CFD has demonstrated its usefulness and reliability for predicting flow quantities; optimization techniques have shown an interesting capability to find optimal solutions for complex problems. Among optimization techniques available today, evolutionary algorithms[7–9] are preferable to other local methods because they have been shown to be powerful tools in handling multimodal, nonconvex, and multiobjective problems. Gradient-based optimization methods are still in use only for special quadratic cases.

Until now, however, the use of evolutionary techniques in combination with CFD codes for solving multiobjective optimization problems in compressor aerodynamics has been limited by the tremendous computational effort required. Because the large majority of the computational time is spent in the evaluation process of the objective function, a faster solution approach to calculate the flowfield would be more appropriate. From this point of view, the use of Euler solvers with an integral boundary-layer approach are more desirable than Navier–Stokes codes, at least to predict flow quantities in the vicinity of the design point of the machine. On the other hand, the available evolutionary optimization techniques are not effective enough in exploiting information from a population of candidate solutions to the optimization problem, so that the number of generations required to get the optimum is usually great, thus penalizing the convergence process.

In this paper, a powerful evolutionary optimization code is presented to support the development of a new generation of optimal airfoils for axial compressors. The scope of the optimization is to maximize both aerodynamic efficiency and pressure rise of subsonic cascades. The optimization code is carried out by the combination of a geometry code for the airfoil description, a blade-to-blade inviscid/viscous solver, and a numerical evolutionary algorithm featuring a novel evaluation technique.

Scope of the Design Optimization

The ultimate goal of compressor design is to create a blade with maximum pressure rise and minimum total pressure loss, along with an acceptable tolerance to incidence angles variations. A number of different design choices can be carried out to reach this goal. When a cascade of airfoils is considered, the flow may be turned by a high cambered profile at low incidence angles or, equivalently, by a low cambered profile having marked positive incidence. In this respect, the shape of the profile plays an important role because it affects the nature of the boundary layer on the suction side and, therefore, the amount of profile losses. On the other hand, the designer may use a high solidity cascade to decrease the aerodynamic loading on a single profile, thus reaching the maximum pressure rise with the whole blade row, or may adopt a low solidity cascade to minimize the friction losses for a prescribed pressure rise. All of these choices involve a decision-making process that makes the design a challenging task.

In a compressor cascade, the pressure rise is achieved by enthalpy exchange from the dynamic head (relative or absolute, according to the type of motion) and can be calculated using the following nondimensional pressure ratio (PR) (Fig. 1):

$$\mathrm{PR} = \bar{p}_2/p_1 \tag{1}$$

On the other hand, the total pressure loss coefficient can be defined using the following equation:

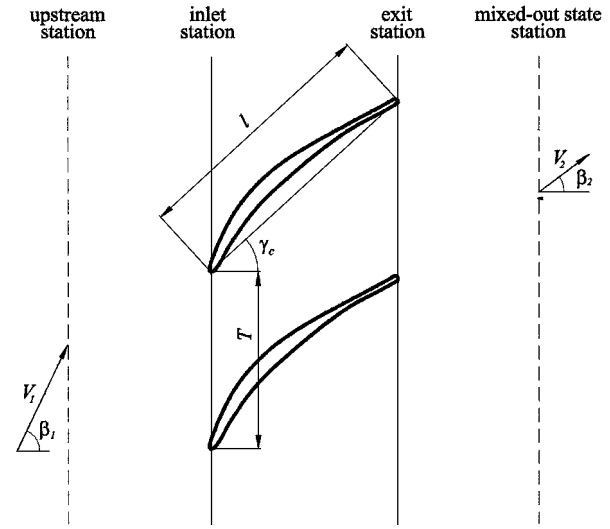

Fig. 1 Two-dimensional cascade geometry for axial flow compressors.

$$\omega = \frac{p_{02}^{\mathrm{is}} - \bar{p}_{02}}{p_{01} - p_1} \tag{2}$$

where the superscript is denotes the final isentropic state of the thermodynamic process. In the preceding equations, the actual static pressure downstream of the cascade is calculated according to the mixed-out state hypothesis.[10] According to this hypothesis, the implicit state of the flow in an arbitrary plane downstream of the cascade is obtained analytically from the known stagnation conditions, mass flow rate, and angular momentum:

$$\bar{\rho}\bar{u}Tb = \int \rho u b r \, \mathrm{d}\theta = \dot{m}$$

$$(\bar{\rho}\bar{u}^2 + \bar{p})Tb = \int (\rho u^2 + p) b r \, \mathrm{d}\theta = \int \left(u + \frac{p}{\rho u}\right) \mathrm{d}\dot{m} - \rho_e V_e u_e \Theta b + \frac{p_e \delta^* b V_e}{u_e}$$

$$\bar{\rho}\bar{u}\bar{v}Tb = \int \rho u v b r \, \mathrm{d}\theta = \int v \, \mathrm{d}\dot{m} - \rho_e V_e v_e \Theta b \tag{3}$$

where T is the pitch and $V = \sqrt{(u^2 + v^2)}$ is the speed. Θ and δ^* are the momentum thickness and the displacement thickness of the boundary layer at the cascade exit plane. The mixed-out quantities in Eq. (3) can, thus, be used to calculate the Mach number and the total pressure at the station downstream:

$$\bar{M}_2^2 = (\bar{\rho}_2/\gamma\,\bar{p}_2)\left(\bar{u}_2^2 + \bar{v}_2^2\right)$$

$$\bar{p}_{02} = \bar{p}_2\left\{1 + [(\gamma - 1)/2]\bar{M}_2^2\right\}^{\gamma/(\gamma - 1)} \tag{4}$$

The determination of the maximum pressure rise that can be achieved in a compressor cascade is vital in the design of high-performance axial-flow compressors. As the pressure rise increases for a given inlet flow angle, the profile tends to become more cambered or to have higher incidence angles and, thus, to have a suction side more exposed to flow separation due to the adverse pressure gradients. In these circumstances, the total pressure losses generated inside the boundary layer, in the wake, and in separated flow regions become remarkable, and they quickly convect in the mean flow. Moreover, the high-pressure rise associated with large turning at high inlet angles promotes turbulent separation so that the stall angle of attack moves progressively closer to the design value when section camber increases. Therefore, both pressure rise and total pressure loss are linked in such a way that the improvements obtained in one of the two significantly affect the other. In other words,

a conflict appears between the two objectives of the design, so that a tradeoff between pressure rise and efficiency is unavoidable.

The aim of the optimization problem presented here is to maximize the two-objective function:

$$\boldsymbol{F}(\boldsymbol{x}) = (f_1, f_2) = (\mathrm{PR}, 1-\omega) \tag{5}$$

where $\boldsymbol{x}$ is the vector the unknown optimization parameters or decision variables of the design.

Geometry Description

The profile geometry is described using parametric curves. As shown in Fig. 2, the shape is parameterized using two Bezier curves (one for the pressure side and one for the suction side). Each curve is defined by $n+1$ control points constituting the Bezier polygon. Therefore, the general expression for the Cartesian coordinates of the pressure side and the suction side is

$$\begin{Bmatrix} x(t) \\ y_{\mathrm{ps}}(t) \\ y_{\mathrm{ss}}(t) \end{Bmatrix} = \sum_{i=0}^{n} C_{n,i} t^i (1-t)^{n-i} \begin{Bmatrix} x(i) \\ y_{\mathrm{ps}}(i) \\ y_{\mathrm{ss}}(i) \end{Bmatrix} \tag{6}$$

where $t \in [0, 1]$ is the nondimensional parameter of each curve and $C_{n,i}$ are coefficients defined as

$$C_{n,i} = n!/i!(n-i)! \tag{7}$$

The control points' coordinates on the airfoil contour are defined by the following equations:

$$x(i) = \begin{cases} 0, & \text{if} \quad i = 0 \\ (i-1)/(n-2), & \text{if} \quad 0 < i < n \\ 1, & \text{if} \quad i = n \end{cases} \tag{8}$$

$$[y_{\mathrm{ps}}(i),\, y_{\mathrm{ss}}(i)] = \begin{cases} 0, & \text{if} \quad i = 0 \quad \text{or} \quad i = n \\ y_{\mathrm{cl}}(i) \mp \delta(i), & \text{if} \quad 1 < i < n-1 \\ \delta(i), & \text{if} \quad i = 1 \quad \text{or} \quad i = n-1 \end{cases} \tag{9}$$

where $y_{\mathrm{cl}}(i)$ and $\delta(i)$ are the ith components of the primary control points, that is, the parameter set of the optimization for profile geometry (Fig. 2). This method is inspired by the well-known practice of combining a camber line with a thickness distribution superimposed to the camber line. This method is effective in avoiding the creation of useless profiles that would come from the intersection of the pressure and the suction surface if these were defined separately. The leading-edge and trailing-edge curvatures are described by control points lying on the $x = 0$ and 1 axes, respectively. When this method is used, the direction of the camber line at the leading and the trailing edge can be well approximated by

$$\theta_{\mathrm{inl}} = \frac{y_{\mathrm{cl}}(1)}{x(2)}, \qquad \theta_{\mathrm{out}} = \frac{y_{\mathrm{cl}}(n-1)}{x(n) - x(n-1)} \tag{10}$$

so that the incidence angle $\alpha_1 = \beta_1 - \theta_{\mathrm{inl}}$ can be easily specified.

In the present study, the decision variables are 1) airfoil shape parameters $n = 6$ (Fig. 2), 2) chord length l, 3) pitch T, and 4) incidence angle α_1.

Constraints

When optimization problems are solved, it is important to search for feasible optima. The condition of feasible optimality can be obtained using appropriate constraints. Because the number and the type of constraints strongly affect the nature of the optima, the use of specific limiting conditions must be carefully studied, and their effects possibly predicted a priori. Moreover, appropriate constraint-handling techniques have to be used to discriminate between feasible and infeasible solutions.

Some authors imposed constraints on the maximum airfoil thickness and on the area delimited by the airfoil pressure and suction sides[3,11] and used suitable penalty functions to handle them. However, such constraints do not necessarily lead to feasible airfoils, especially from a structural point of view, because the geometric properties of an airfoil are not globally defined only by the maximum thickness and the contour area. Nevertheless, they are useful to make comparison with existing airfoil geometries in retrofitting design problems.

Recently, Köller et al.[5] used a functional constraint on the complete operating range of a compressor cascade and included it in a single-objective function of the optimization using a heuristic factor. Benini and Toffolo[12] showed how to constrain the flow turning angle of decelerating cascades using exponential penalty functions.

In this work, a constraint on the operating range of the profile was adopted, and no conditions on the structural properties of the airfoil were considered. As is well known, the operating range of a compressor cascade can be defined as the interval of incidence angles for which the total pressure loss ω doubles its minimum value or, alternatively, the value chosen as a reference for the design, ω^*. To include the operating range as a constraint, the latter criterion was adopted. For a generic cascade, the total pressure loss was measured in five operating conditions defined by $\beta_1 - \beta_1^* = 0, \pm 2.5, \pm 5$ deg (as shown in Fig. 3) and compared to that of the design. To satisfy the constraint, the following condition had to be verified at each operating point i:

$$\omega_i/\omega^* \le 2 \qquad \forall i = 1, \ldots, 5 \tag{11}$$

The constraint on the operating range has an incisive impact both on fluid dynamic and structural aspects. It is primarily useful for

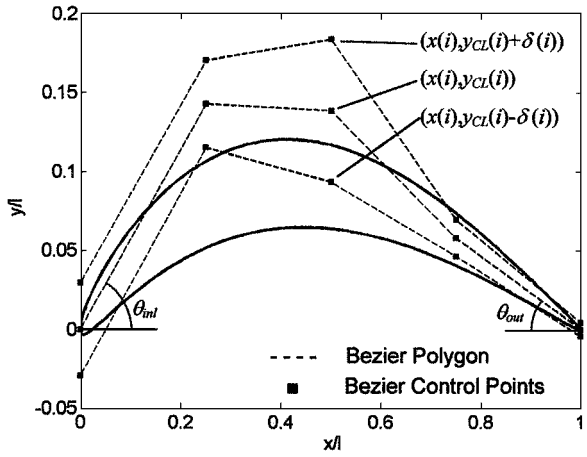

Fig. 2 Geometry parameterization of an airfoil using Bezier curves, squares are control points of Bezier curves.

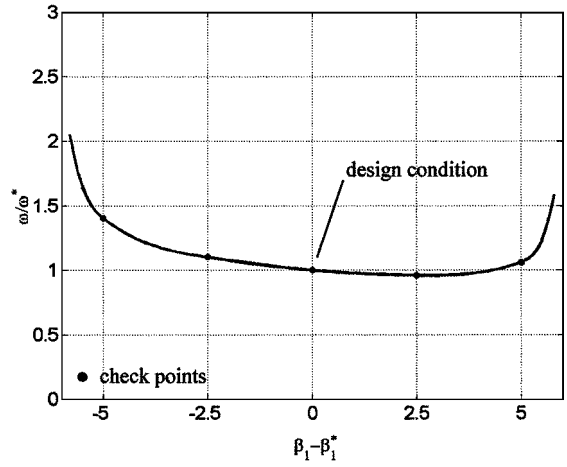

Fig. 3 Total pressure loss as function of inlet flow angle at the design point, dots are the sampled points considered in constraint evaluation.

determining an acceptable stall/surge margin of the compressor. Moreover, it controls indirectly the shape of the leading edge by making it sufficiently rounded and regular and addresses the geometry search toward profiles having adequate structural strength. Such a condition is definitely useful in governing the maximum thickness of the profile without explicit constraints that would limit the exploration of nonconventional solutions within the design space.

Multiobjective Evolutionary Algorithms

Multiobjective Optimization and Pareto Concepts

In multiobjective optimization problems, the simultaneous accomplishment of a number of different and often conflicting criteria is required. These objectives can be seen as distinct measures of performance of the system to be optimized and may be (in)dependent and/or incommensurable.

A multiobjective optimization problem is mathematically defined as the maximization of the components of a vector $\boldsymbol{F}(\boldsymbol{x}) = [f_1(\boldsymbol{x}), f_2(\boldsymbol{x}), \ldots, f_m(\boldsymbol{x})]$, where $\boldsymbol{F}$ is the evaluation function that maps the candidate solutions in the decision variable space [such as $\boldsymbol{x} = (x_1, \ldots, x_n)$] to the performances in the objective function space (Fig. 4). It is very difficult to establish a priori whether a global optimal solution to a multiobjective optimization problem exists or not. In fact, problems having a combination of decision variables values that maximizes all of the components of vector $\boldsymbol{F}$ simultaneously are hard to find among real-world engineering problems: they generally show a (possibly uncountable) set of solutions, whose corresponding performances represent the optimal tradeoffs in the objective function space.

The search toward these optimal tradeoffs among the objectives is driven by a key concept in multiobjective optimization: Pareto optimality. This concept is used to establish a hierarchy among the solutions by comparing the performances scored in the single-objective functions. First, the definition of Pareto dominance must be introduced: a vector $\boldsymbol{u} = (u_1, \ldots, u_m)$ in the objective function space is said to dominate $\boldsymbol{v} = (v_1, \ldots, v_m)$ if and only if all of the components of $\boldsymbol{u}$ are greater or equal to the ones of $\boldsymbol{v}$ and at least one component of $\boldsymbol{u}$ is strictly greater than the corresponding one in $\boldsymbol{v}$. Then a solution $\boldsymbol{x} = (x_1, \ldots, x_n)$ of a multiobjective optimization problem is said to be Pareto optimal with respect to the entire decision variable space if and only if there is no other solution $\boldsymbol{x}'$ for which $\boldsymbol{F}(\boldsymbol{x}') = [f_1(\boldsymbol{x}'), \ldots, f_m(\boldsymbol{x}')]$ dominates $\boldsymbol{F}(\boldsymbol{x}) = [f_1(\boldsymbol{x}), \ldots, f_m(\boldsymbol{x})]$ (Fig. 5).

The set of Pareto optimal solutions, which coincides with the set of the optimal tradeoffs among the objectives, is also called the Pareto optimal set, and the set of the corresponding vectors in the objective function space is called the Pareto front.

Evolutionary Algorithms for Solving Multiobjective Optimization Problems

The solution of a multiobjective optimization problem requires 1) finding solutions close to the true Pareto optimal set and 2) spreading solutions over the entire Pareto optimal set, finding combinations of decision variables that are widely different from each other, and introducing no bias toward any particular objective.

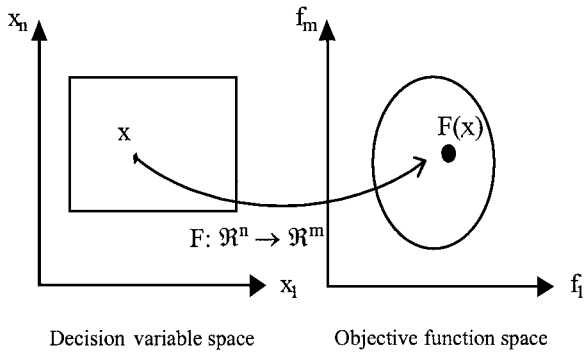

Fig. 4 Representation of a multiobjective optimization problem.

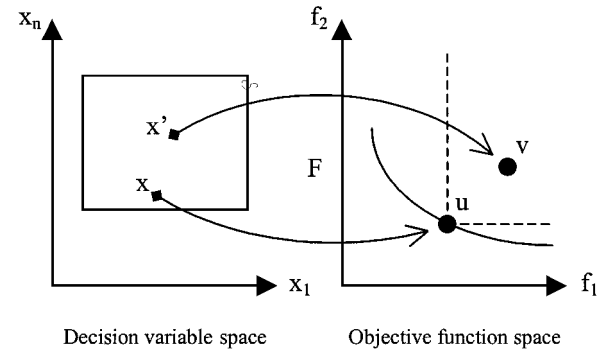

Fig. 5 Pareto dominance and Pareto optimality.

Classical search and optimization methods are destined to fail when facing multiobjective optimization problems with Pareto's approach mainly because they are unable to find multiple solutions in a single run, and they have to be applied as many times as the number of Pareto optimal solutions required. Moreover, there is no guarantee that the solutions found through the repeated application of these methods are spread enough over the Pareto optimal set. Such issues arise, for example, using the linear objective function aggregation technique[5]: a virtual objective function is built by weighting the original objective functions, through priority coefficients, but only a single solution can be determined for each virtual objective function, and the priority coefficients have to be varied to find other solutions.

Pareto's approach to multiobjective optimization was instead implemented in a straightforward way by the class of search algorithms known as multiobjective evolutionary algorithms (MOEAs). MOEAs have been developed over the past decade, and severe tests on complex mathematical problems as well as on real-world engineering problems have shown that they can remove the cited difficulties faced by classical methods.

An evolutionary algorithm uses both stochastic and deterministic elements and aims at imitating aspects of the natural evolution of biological organisms: the artificial evolution process starts with a randomly initialized population of individuals (a set of points in the search space) that evolves following the Darwinian principle of the survival of the fittest. New generations of solutions are created using some simulated evolutionary operators, such as crossover and mutation: the probability of survival for each individual depends on its fitness, that is, on how well it performs with respect to the objective(s) of the optimization problem.

Because MOEAs use a population of solutions during the search, a single run will find many Pareto optimal solutions; moreover, by adding a diversity-preserving mechanism to the algorithm, solutions can be widely spread over the Pareto optimal set.

Genetic Diversity Evaluation Method

An MOEA without a diversity-preserving mechanism would prematurely converge toward the first few Pareto optimal solutions found; therefore, a technique that aims at the maintenance of genetic diversity within the population must be included in the basic scheme of the evolutionary algorithm.

A number of different methods have been proposed to perform the task: they usually promote the formation of stable subpopulations, called niches, along the Pareto optimal set, introducing some modifications to the selection and/or replacement process. See Deb[9] for an up-to-date review of the subject, in particular Srinivas and Deb's Nondominated Sorting Genetic Algorithm and Zitzler and Thiele's Strength Pareto Evolutionary Algorithm. These methods have been widely tested and successfully applied, but their performance is affected by the definition of arbitrary parameters that are difficult to be set without prior knowledge of the objective function space.

Recently, a new diversity-preserving method, the Genetic Diversity Evaluation Method (GeDEM), has been developed by Toffolo and Benini.[13] The GeDEM does not follow the tradition of niching methods, such as the fitness sharing technique and its numerous

variants, but intends to make a compromise between the fundamental tasks of a search algorithm: the exploration of the search space and the refinement of the search around the most promising regions. The method was inspired by the consideration that an efficient exploration of the search space and the preservation of genetic diversity within the population are clearly connected; however, the mutation operator alone is not suitable for these tasks because it tends to produce low-ranked individuals, which are immediately rejected or have very poor mating chances. The evaluation method should emphasize not only the best-ranked individuals, but also the ones that are much different from the rest of the population, that is, the individuals that are necessary to keep alive the exploration of the search space. Thus, a two-objective evaluation is needed to combine these needs. After the usual evaluation of the individuals through the objective functions, the GeDEM performs an additional evaluation step considering a measure of genetic diversity as an objective of a two-criteria optimization problem, the other objective being the Pareto rank scored in the objectives of the original optimization problem. Then, the GeDEM once again ranks the solutions according to the concept of Pareto optimality, with slight modifications that are introduced to consider the special case of solutions having the same rank in the objectives of the original optimization problem.

Optimization Tools

Blade-to-Blade Code

Flow quantities were calculated using the MISES solver developed at the Massachusetts Institute of Technology.[14] MISES is a collection of programs for cascade design and analysis for compressible viscous flows over an arbitrary quasi-three-dimensional cascade of airfoils. (It was originally developed for airfoils, and later it was reprogrammed to allow cascade analysis.) In this code, a zonal approach is used to solve the viscous flow indirectly, and an equivalent inviscid flow is postulated outside a displacement streamline that includes the viscous layer. The equivalent inviscid flow is defined as locally irrotational and containing all of the mass flow. The viscous effects are modeled using the mass flow defect. The inner boundary of the equivalent inviscid flow is displaced outward from the wall by the displacement thickness of the boundary layer. The outer inviscid flow is solved using the steady-state Euler equations, and the boundary-layer flow is solved using an integral boundary-layer method. MISES uses a modified Abu-Ghannam/Shaw transition criterion (see Ref. 15) to predict the transition region of the boundary layer from laminar to turbulent. The outer flow is coupled with the boundary-layer flow through the edge velocity and density. Because the inviscid and viscous solutions are fully coupled and solved simultaneously, flows involving separation can be calculated. However, it can handle only moderate stall phenomena because, for massive separations, the iteration procedure does not converge. The influence of the stream tube height is taken into account, and for local supersonic regions the artificial viscosity formulation is implemented. Flow quantities of interest, such as exit flow angle, pressure rise, and total pressure loss, are calculated using the equations of mass, momentum, and energy conservation. Structured grids (I type and H type) with elliptic smoothing are employed for space discretization. Figure 6 shows an example of a computational I-type grid for subsonic compressor cascades that was used in the present study.

Validation of the Blade-to-Blade Code

Because the validity of the optimization process depends mainly on the precision of flow computations, an extensive validation of the blade-to-blade code was carried out. For this purpose, comparisons between available experimental data, as test cases in the open literature, and MISES calculations were performed. Such an investigation was useful to assess the reliability of the code for computing the flow quantities relevant to the optimization process. In particular, pressure and Mach number distribution on the blade contour, pressure rise, total pressure losses, and flow turning were considered for validation.

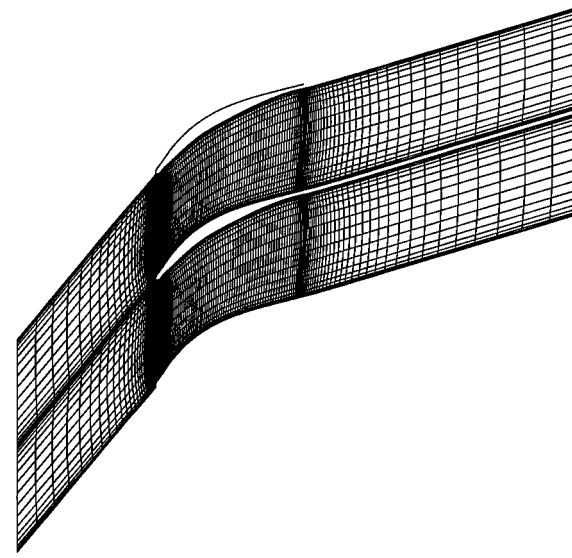

Fig. 6 I-type grid used in simulations of compressor cascades.

Figure 7 shows pressure and Mach number distribution on the pressure and the suction side of a NACA 65 cascade of airfoils at low speed having $\beta_1 = 30$ deg, $\sigma = 1$, and axial velocity density ratio (AVDR) $= 1.0$, for $\alpha = 18$ and 24 deg. The computed values exhibit good agreement with experimental data.[16] The values of PR, total pressure losses, and flow turning were compared with experimental values, as well for a large number of incidence angles. The results obtained are regarded as satisfactory in all of the conditions explored during the validation.

Optimization Code

The structure of the MOEA used in the present work follows the main steps of a $\mu + \mu$ evolution strategy[8] (Fig. 8). However, decision variables are coded in binary strings, as is usually done in genetic algorithms.

In the first step, parents' selection is performed, each individual having the same probability of being chosen. (The actual struggle for survival occurs after the evaluation step, when only μ individuals survive among the $\mu + \mu$ available.) Then parents enter the reproduction step, generating μ offspring through a crossover strategy. Some bits of the strings coding the decision variable values of the offspring are also randomly mutated with a probability p_{mut}. The whole population of $\mu + \mu$ individuals is also checked for possible clones. Clones are then destroyed and replaced with new randomly generated individuals, to encourage the exploration of the search space and to give the GeDEM a clearer picture of the actual genetic diversity within the population. The objective function values of the μ offspring are then evaluated, and there is a Pareto ranking of the $\mu + \mu$ individuals according to Goldberg's scheme,[7] by which the population is divided into waves of individuals having different ranks, each wave dominating the others with a lower rank. The whole population of $\mu + \mu$ individuals is also processed to determine its genetic diversity. In this algorithm, the chosen measure of genetic difference assigned to an individual is the minimum normalized Euclidean distance in the decision variable space from another individual. The next step of the algorithm is the application of the GeDEM: a new Pareto ranking is performed on the $\mu + \mu$ solutions, using as objectives the ranks obtained during the evaluation step, that is, according to the objectives of the original optimization problem, and the measure of diversity. Following these two criteria, the μ best-ranked solutions, which are also selected to survive, are the optimal tradeoff between the best ranked in the original objectives and the most different. Finally, the number of generations elapsed is compared to the established maximum number of generations: If this termination condition is met, the process stops; otherwise, the surviving solution become the starting population for the next generation.

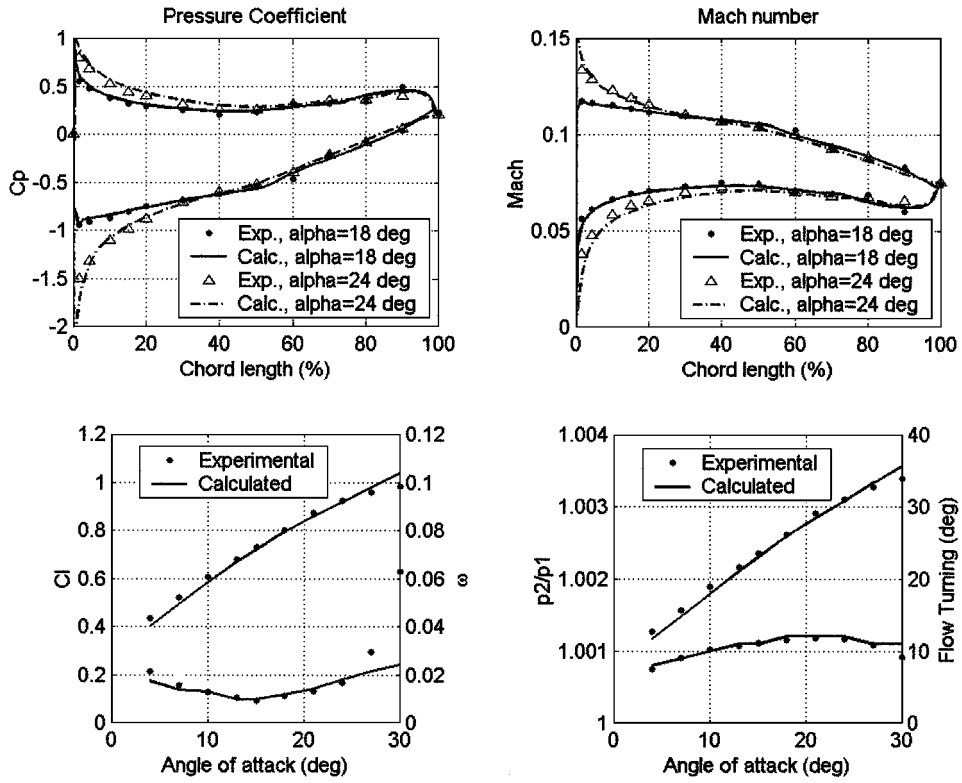

Fig. 7 Results of the MISES code validation.

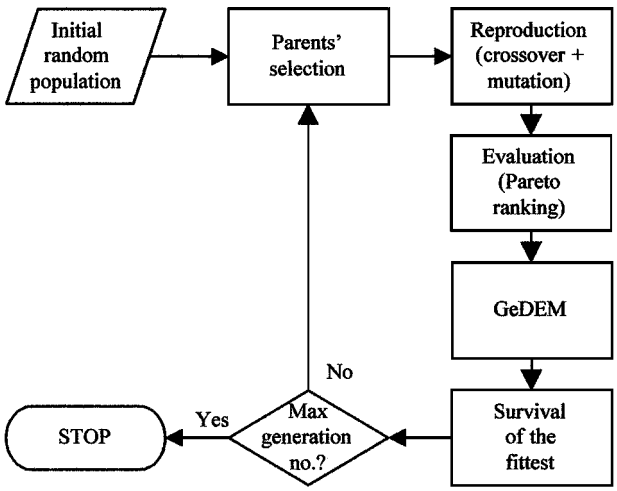

Fig. 8 Scheme of MOEA used in the present work.

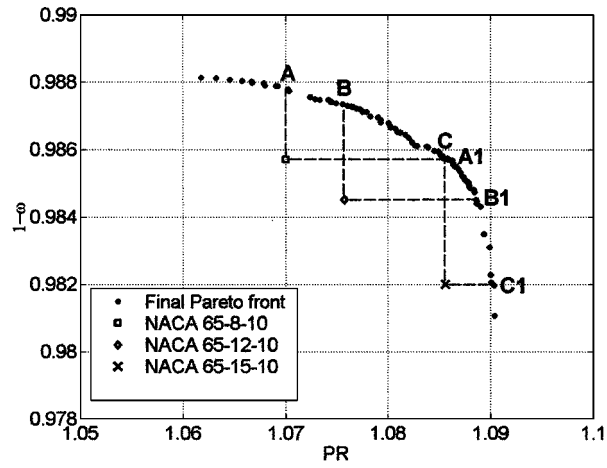

Fig. 9 Final Pareto front of the optimization compared with performance figures of NACA 65 cascades.

Family of Optimized Profiles

To demonstrate the effectiveness of the design tool presented in the preceding sections, a family of optimized profiles was created as follows.

The well-known family of NACA 65-series of cascades for axial flow compressors was considered as reference. The profiles belonging to this family cover, for a given inlet flow angle β_1 and AVDR, a wide range of flow turning angles. The fluid dynamic inlet boundary conditions, $M_1 = 0.5$, $Re_1 = 10^6$, and $\beta_1 = 45$ deg, as well as the cascade chord length, $l = 104.7$ mm, and solidity, $\sigma = 1$, were fixed, and among the configurations available for that class of profiles, the geometries of NACA 65-8-10, NACA 65-12-10, and NACA 65-15-10 were chosen. The performances of these geometries were measured numerically for many values of the angle of attack.

The purpose here was to improve on the performances of the above mentioned NACA 65 profiles using the optimization process described in the preceding sections, with the aim of obtaining a new family of profiles that dominates, under the aforementioned boundary conditions, the reference one with respect to both efficiency and pressure rise. Because of the constraint formulation adopted, the operating range of the new profiles was also required to be at least as large as that of the reference profiles.

Figure 9 shows the Pareto front obtained with 100 individuals after 200 generations. The calculated performances of NACA 65 profiles are reported as well. The leftmost part of the Pareto front includes the profiles having maximum efficiency and lower PR; the rightmost part includes those having maximum PR and lower efficiency. The values of $1 - \omega$ found by the optimization procedure range from $(1-\omega)_{\min} = 0.981$ to $(1-\omega)_{\max} = 0.988$ as the pressure rise ranges from $(\mathrm{PR})_{\max} = 1.09$ to $(\mathrm{PR})_{\min} = 1.068$. The shape of the Pareto front confirms that at low PR it is possible to increase profile loading without penalizing the efficiency in a very significant way; on the other hand, as the flow turning moves toward its maximum, a sudden drop in the profile efficiency is unavoidable.

Table 1 Performances of reference and optimized cascades

Cascade of profiles	PR	ΔPR, %	ω	$\Delta\omega$, %
NACA 65-8-10	1.070	——	0.0143	——
A	1.070	0	0.0123	−14
A1	1.086	+1.5	0.0143	0
NACA 65-12-10	1.076	——	0.0155	——
B	1.076	0	0.0127	−19
B1	1.089	+1.2	0.0155	0
NACA 65-15-10	1.086	——	0.0180	——
C	1.086	0	0.0142	−21
C1	1.090	+0.4	0.0180	0

Note that the individuals belonging to the Pareto front dominate the cascades of NACA 65 profiles. In particular, the cascade of NACA 65-8-10, NACA 65-12-10, and NACA 65-15-10 are dominated by individuals A, B, and C with respect to profile efficiency (PR being fixed) and by individuals A1, B1, and C1 with respect to PR (profile efficiency being fixed). The superiority of the new profiles was quantified, and the results are summarized in Table 1.

The reasons why the new cascade of profiles behave better than the reference profiles are discussed in the following section, which provides a physical interpretation of the results obtained.

Discussion of Results

Before going into details, a preliminary consideration on the tools used to interpret the results is given.

When the method of analysis proposed by Denton[17] is followed, the two-dimensional loss in a compressor cascade may be schematically divided into two components: the blade boundary-layer loss and the trailing-edge (or mixing) loss. The former includes the effect of boundary-layer growth on the pressure and suction sides of the airfoil and is related to viscous dissipation by shear work in the boundary layers, where velocity gradients are remarkable. The latter comes from contributions of shear strains that occur in the wakes or at the edge of separated flow, that is, typically downstream of a blade. See Denton[17] for a complete treatment of this subject; here the purpose is to recall briefly the main aspects of that analysis to provide the basis for a physical interpretation of results.

Once the cascade solidity, inlet Mach number, and flow inlet angle have been fixed, the principal factor determining the loss production of a laminar or turbulent boundary layer is the cube of the ratio of the freestream velocity to the flow velocity at cascade inlet. The effect of suction surface is the dominant in producing loss because the highest peak of freestream velocity takes place on it, in the proximity of the leading edge. Another important factor influencing the loss production in the boundary layers is the location of the transition point from laminar to turbulent because the dissipation coefficient undergoes a rapid increase from that point. These dependencies suggest that keeping the peak velocity low, maintaining the laminar boundary layer, and decelerating quickly the turbulent flow are decisive aspects for minimizing the blade boundary-layer loss.

On the other hand, the trailing-edge loss is basically determined by three factors: the low base pressure effect located at the trailing edge, the mixed-out loss of the boundary layers just before the trailing edge, and combined blockage of the trailing edge and the boundary layers. For nearly sharp trailing edges, as those considered in this work, the magnitude of the trailing-edge loss depends mainly on the total momentum thickness and on the square of the total displacement thickness of the boundary layers at the trailing edge.

As a result, the comparison between the Mach number distribution on the profile surfaces of reference and optimized cascades, as well as the analysis of computed boundary-layer properties, may give rigorous justifications about the reason for improved performances. In the following sections, the reference cascades of profiles NACA 65-8-10, NACA 65-12-10, and NACA 65-15-10 are compared with the optimized ones, A, B, C, A1, B1, and C1, according to such criteria.

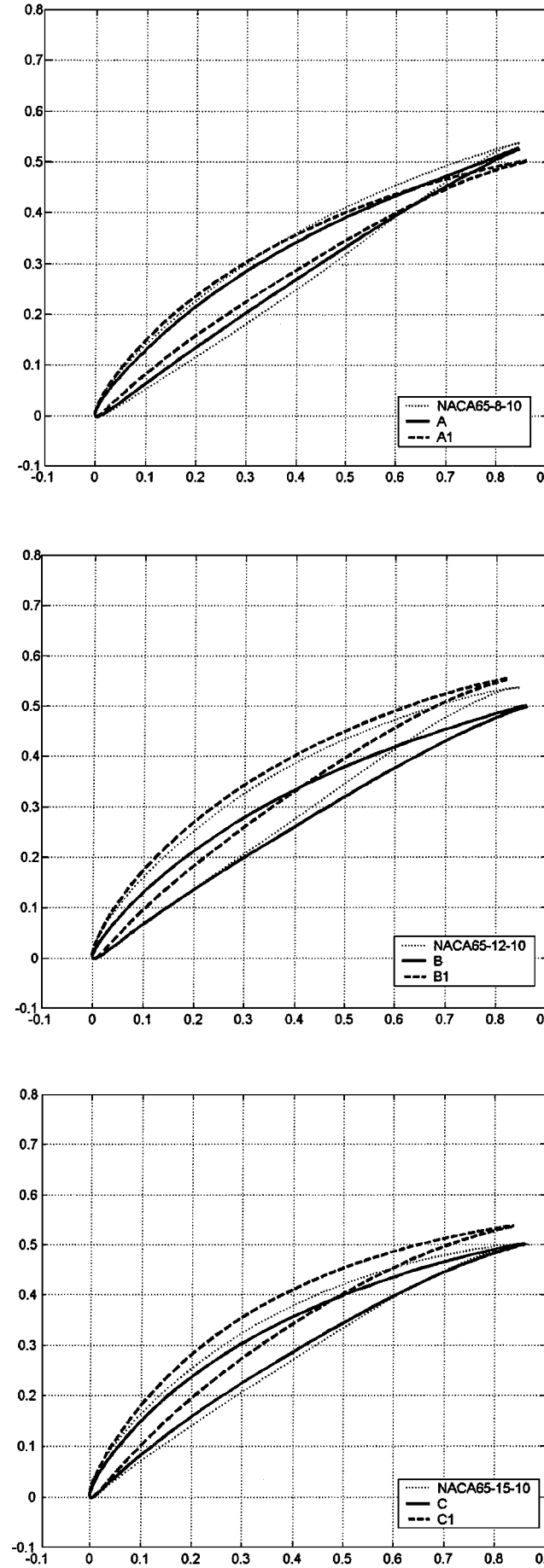

Fig. 10 Shapes of reference NACA 65 profiles compared with those optimized for efficiency and PR.

Comparison Between Reference and Optimized Cascades

The presentation of the results is organized in the following way: For each NACA cascade considered in this paper, the flow characteristics of the reference configurations are compared to both PR-optimized and efficiency-optimized configurations.

The profile shapes are compared in Fig. 10. The computed pressure coefficient and Mach number distribution are given in Figs. 11–13 at different incidence angles, whereas the same quantities are compared in Fig. 14 at the optimal incidence of each profile. The computed boundary-layer properties relevant to the discussion are given in Table 2. The PR and total pressure loss over the operating range are shown in Fig. 15 for the optimization results regarding NACA 65-8-10.

High-Efficiency Profiles

When the analysis presented in the preceding sections is used, the contribution of blade boundary-layer and trailing-edge loss are highlighted in both design and off-design conditions.

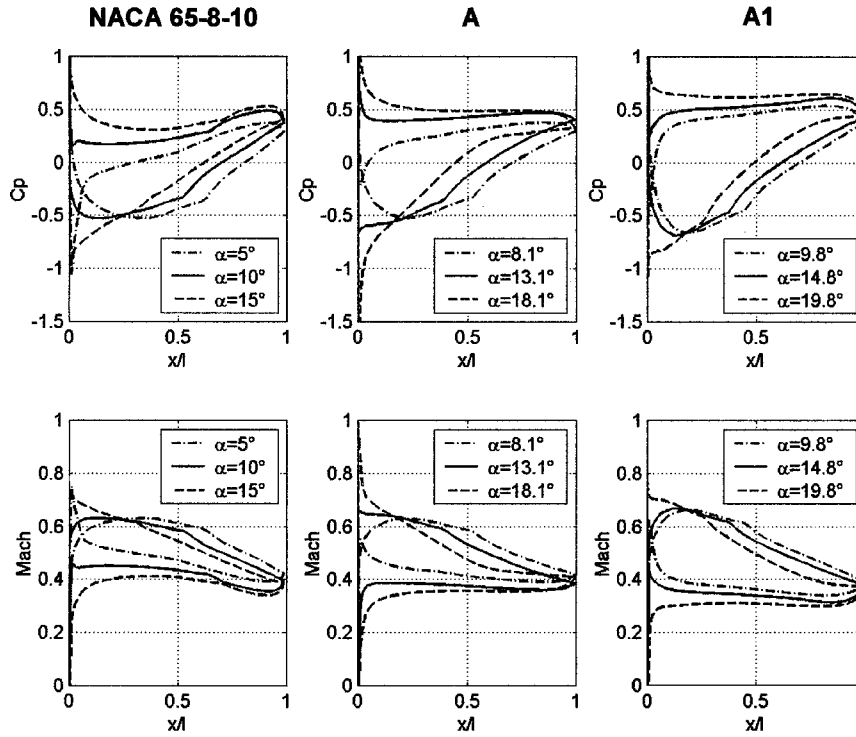

Fig. 11 Computed pressure coefficient and Mach number distribution on reference profile NACA 65-8-10 and optimized profiles, A for maximum efficiency and A1 for maximum pressure recovery, over the operating range.

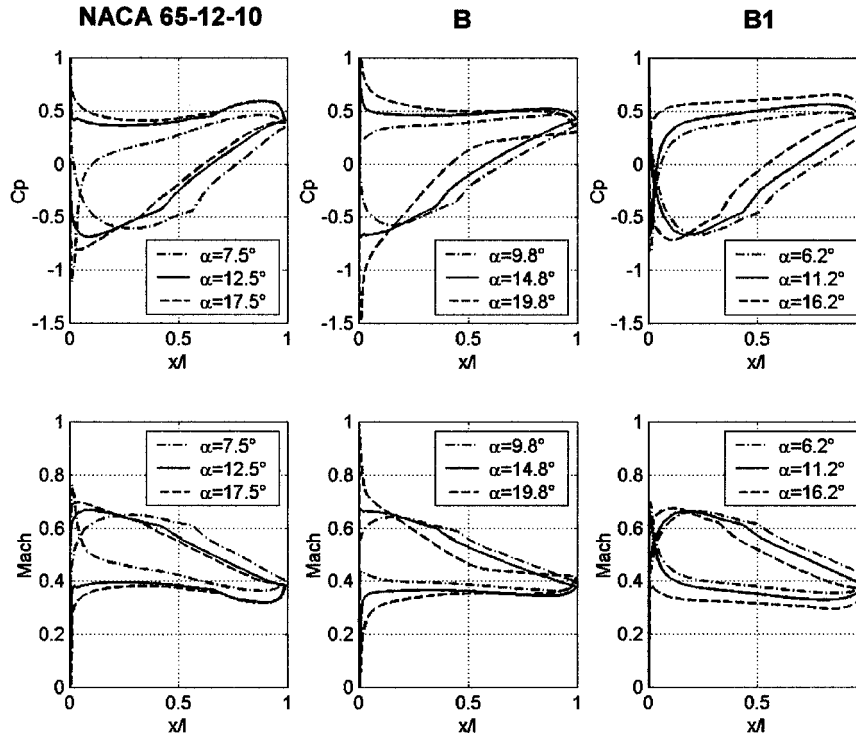

Fig. 12 Computed pressure coefficient and Mach number distribution on reference profile NACA 65-12-10 and optimized profiles, B for maximum efficiency and B1 for maximum pressure recovery, over the operating range.

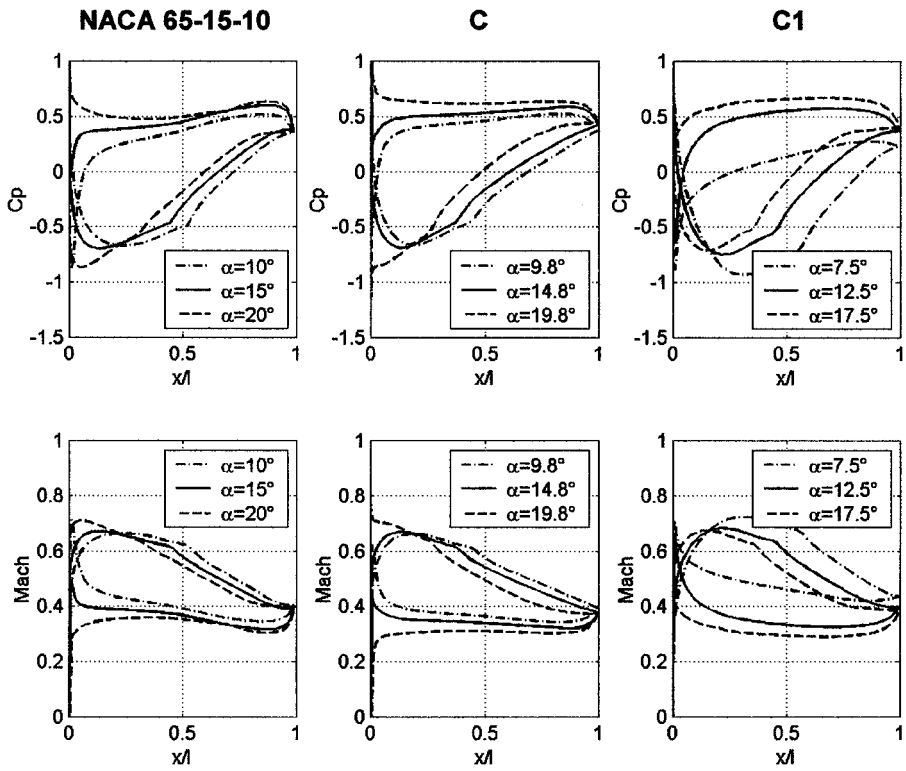

Fig. 13 Computed pressure coefficient and Mach number distribution on reference profile NACA 65-15-10 and optimized profiles, C for maximum efficiency and C1 for maximum pressure recovery, over the operating range.

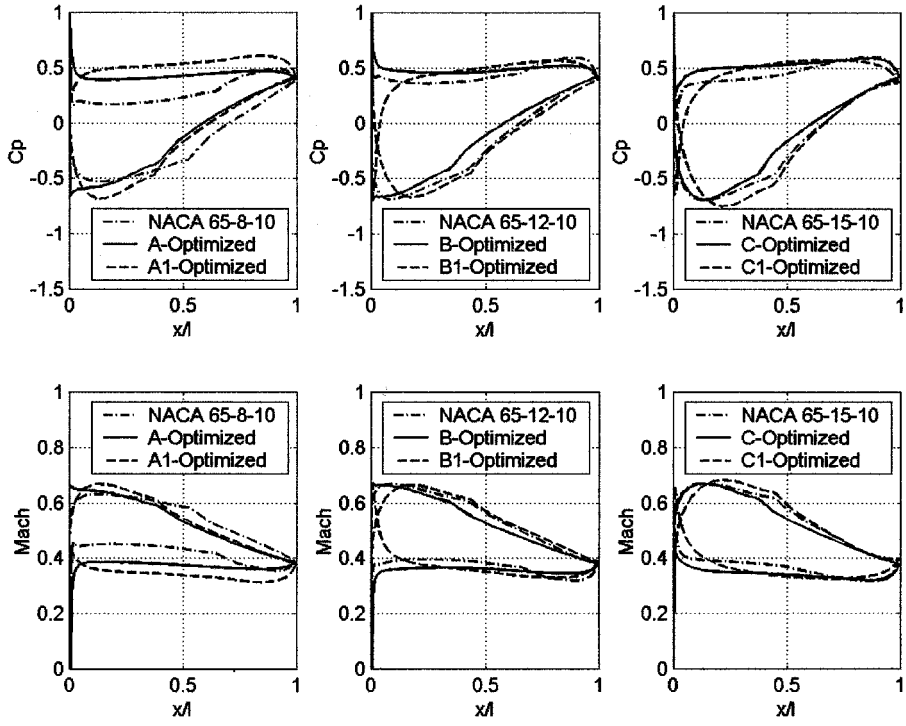

Fig. 14 Computed pressure coefficient and Mach number distribution on reference profiles NACA 65-8-10, NACA 65-12-10, and NACA 65-15-10 and optimized profiles A, B, and C for maximum efficiency and A1, B1, and C1 for maximum pressure recovery at respective optimum incidence.

In design conditions, the Mach number distribution on the profile A shows significant differences with respect to that on NACA 65-8-10. Because the loss production depends on the cube of local freestream velocity, the Mach number distribution on the suction surface must be considered in particular. The peak value of Mach number is almost equal in both cases, $M_{\max} \approx 0.65$, but on A, it is located much closer to the leading edge. This has been studied quite extensively in the past because it regularly happens in controlled diffusion blades. The rapid acceleration of the flow means that the freestream velocity becomes very high when the laminar boundary layer has just started to appear, so that loss production may be considerable in early stages of the following turbulent boundary layer. In the present case, however, the deceleration profile beyond the peak velocity indirectly leads to low losses for the following reasons. First, the NACA chord fraction were $(M/M_1) > 1$ is greater than in A. Second, despite that the region of NACA laminar boundary

Table 2 Computed boundary-layer properties

Cascade of profiles	δ^*_{te}/l, %	Θ_{te}/l, %	Transition point x/l on suction side, %	Transition point x/l on pressure side, %
NACA 65-8-10	4.0	1.8	47.0	64.7
A	3.4	1.5	38.7	99.3
A1	4.8	1.9	38.1	65.9
NACA 65-12-10	5.1	1.9	48.0	58.8
B	4.1	1.8	35.1	100
B1	5.3	2.3	42.2	1.6
NACA 65-15-10	8.4	1.9	38.2	67.6
C	4.8	1.8	37.6	76.8
C1	8.1	2.8	44.2	1.2

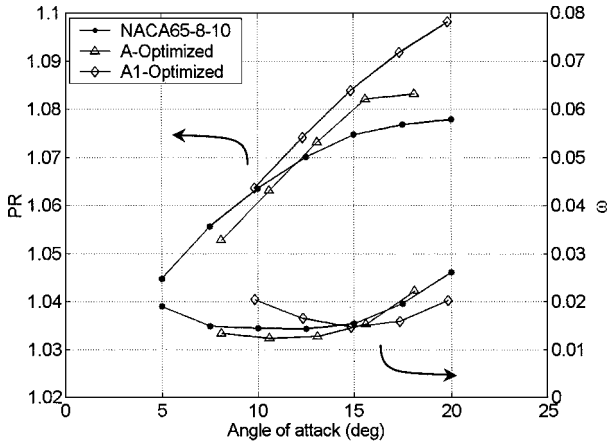

Fig. 15 Computed PR and total pressure loss coefficient on reference profile NACA 65-8-10 and optimized profiles, A for maximum efficiency and A1 for maximum pressure recovery, as functions of angle of attack.

layer is more extended (Table 2), the pressure gradient of A is more favorable for keeping the turbulent skin friction low until the trailing edge. As a result, the integral of loss production over the chord length is lower for the optimized profile. Moreover, both the displacement thickness and momentum thickness at the trailing edge of the suction side are lower (Table 2).

Despite the Mach number distribution on the pressure side having a less important influence on loss production in the blade boundary layer, note that it is relevant in determining the properties of the boundary layer at the trailing edge and, therefore, in establishing the amount of the wake loss. Table 1 indicates that transition does not occur in A, that is, the flow remains laminar over the entire pressure side. This contributes to keep the total displacement thickness and total momentum thickness at the trailing edge very low in comparison to those of the reference NACA profile, with clear benefits on the reduction in the trailing-edge loss.

To summarize, the analysis on profile A indicates that both blade boundary-layer loss and trailing-edge loss are lower under design conditions; this results in lower overall total pressure loss. Very similar conclusions may be drawn for the other efficiency-optimized cascades, and the discussion is qualitatively valid for them as well.

In off-design conditions, the performances of reference and optimized profiles are qualitatively similar due to the constraints used in the optimization process. However, some differences exist and deserve to be highlighted. Figure 15 shows the total pressure loss coefficient and PR for both the reference NACA 65-8-10 and the optimized A cascades as functions of the angle of attack. In general, at high incidences the optimized profiles tend to have a pressure gradient on the suction surface, which increases at the front but decreases remarkably toward the rear, leading to a more continuous deceleration that prevents the boundary layer from separation (Figs. 11–13). At low incidences, NACA profiles exhibit a wider plateau of pressure on the central part of the suction surface; however, they are again characterized by a higher pressure gradient toward the trailing edge. As a result, the new profiles show very satisfactory performances over the entire operating range chosen as a reference (±5 deg in terms of incidence angle variation). Note that the operating range was implemented as an inequality constraint, and therefore, the optimized cascades have at least ±5 deg of tolerance to incidence angle variation.

High-PR Profiles

Once the inlet Mach number and inlet flow angle are fixed, the PR carried out by a cascade depends on flow turning only. Once again the Mach number distribution, as well as the properties of the boundary layer, are very important to understanding the limits of flow deflection and its influence on efficiency.

In design conditions, the reason for the higher PR of optimized cascades, A1, B1, and C1, is apparent because the new profiles carry out higher flow deflections (Fig. 10). As far as the total pressure loss through the cascade is concerned, the new profiles do have the same efficiency as the basic ones; this is a consequence of the balance between lower skin-friction losses (for the same reasons given in the preceding subsection) and higher wake losses (Table 2).

In off-design conditions, the optimized profiles behave well over the whole operating range (Fig. 15). Even at incidence angles very different from the design one, the flow is continuously decelerated toward the trailing edge, keeping the performance of profiles satisfactory.

Conclusions

This paper described a multiobjective optimization method for designing cascades of profiles for subsonic axial flow compressors according to two objectives (maximization of PR and minimization of total pressure loss) under a constraint on the operating range. The method was based on the coupling of a Pareto evolutionary algorithm and a blade-to-blade inviscid/viscous solver.

The capability of the method was demonstrated by developing a new family of optimized cascades that have superior performances to NACA 65 cascades for given inlet boundary conditions $M_1 = 0.5$, $Re_1 = 10^6$, and $\beta_1 = 45$ deg. The superiority is quantified in improvements in the design PR per cascade (from +0.4 to +1.5%) and in the design total pressure loss (from −14 to −21%). The range of incidence angles was constrained at no less than 10 deg.

For high-efficiency profiles, the analysis of the flow on the surface and downstream of it revealed lower blade boundary-layer loss and lower wake loss both in design and off-design conditions, whereas the PR is normally lower as the angle of attack decreases and higher for higher incidences (with respect to NACA cascades).

For high-PR profiles, the results indicated a superiority of the new configurations over the whole operating range, whereas the loss distribution as a function of the incidence is similar to that of NACA profiles and is typically shifted toward higher angles of attack.

By virtue of the robust coupling between the fluid-dynamics code and the evolutionary algorithm, the methodology described is able to carry out a two-objective optimization using 100 individuals in approximately 100 hours CPU time (on a four-processor Compaq AlphaServer ES40, clock frequency 667 MHz). Furthermore, because the code is designed to calculate supersonic and transonic flows, the procedure may well be applied to the optimization of high-speed compressor cascades, even though the reliability of flow calculations and the computational effort must be checked in advance.

References

[1] Hobbs, D. E., and Weingold, H. D., "Development of Controlled Diffusion Airfoils for Multistage Compressor Applications," *Journal of Engineering for Gas Turbine and Power*, Vol. 106, No. 2, April 1984, pp. 271–278.

[2] Behlke, R. F., "The Development of a Second Generation of Controlled Diffusion Airfoils for Multistage Compressors," *Journal of Turbomachinery*, Vol. 108, No. 1, July 1986, pp. 32–41.

[3] Obayashi, S., "Pareto Genetic Algorithm for Aerodynamic Design Using the Navier–Stokes Equations," *Genetic Algorithms in Engineering and Computer Science*, edited by D. Quagliarella, J. Périaux, C. Poloni, and G. Winter, Wiley, New York, 1997, pp. 245–266.

[4]Pierret, S., "Three-Dimensional Blade Design by Means of an Artificial Neural Network and Navier–Stokes Solver," *VKI Lecture Series 1999-02 on Turbomachinery Blade Design Systems*, Brussels, Belgium, 1999.

[5]Köller, U., Mönig, R., Küsters, B., and Schreiber, H.-A., "Development of Advanced Compressor Airfoils for Heavy-Duty Gas Turbines—Part I: Design and Optimization," *Journal of Turbomachinery*, Vol. 122, No. 3, July 2000, pp. 397–405.

[6]Küsters, B., Schreiber, H.-A., Köller, U., and Mönig, R., "Development of Advanced Compressor Airfoils for Heavy-Duty Gas Turbines—Part II: Experimental and Theoretical Analysis," *Journal of Turbomachinery*, Vol. 122, No. 3, July 2000, pp. 406–415.

[7]Goldberg, D. E., *Genetic Algorithms for Search, Optimization and Machine Learning*, Addison Wesley Longman, Reading, MA, 1989.

[8]Schwefel, H.-P., *Evolution and Optimum Seeking*, Wiley, New York, 1995.

[9]Deb, K., *Multi-Objective Optimization Using Evolutionary Algorithms*, Wiley, Chichester, England, U.K., 2001.

[10]Drela, M., and Youngren, H., *A User's Guide to MISES 2.3*, Massachusetts Inst. of Technology, Computational Aerospace Sciences Lab., MIT Press, Boston, MA, 1995.

[11]Dulikravich, G. S., Martin, T. J., Dennis, B. H., and Foster, N. F., "Multidisciplinary Hybrid Constrained GA Optimization," *Evolutionary Algorithms in Engineering and Computer Science*, edited by K. Miettinen, P. Neittaanmäki, M. M. Mäkelä, and J. Périaux, Wiley, New York, 1999, pp. 233–259.

[12]Benini, E., and Toffolo, A., "A Parametric Method for Optimal Design of Two-Dimensional Cascades," *Journal of Power and Energy*, Vol. 215, 2001, pp. 465–473.

[13]Toffolo, A., and Benini, E., "A New Pareto-Like Evaluation Method for Finding Multiple Global Optima in Evolutionary Algorithms," *Proceedings of the Genetic and Evolutionary Computation Conference (GECCO-2000)*, edited by D. Whitley, Las Vegas, NV, USA, July 2000, pp. 405–410.

[14]Giles, M. B., and Drela, M., "Two-Dimensional Transonic Aerodynamic Design Method," *AIAA Journal*, Vol. 25, No. 9, 1987, pp. 1199–1206.

[15]Drela, M., "MISES Implementation of Modified Abu-Ghannam/Shaw Transition Criterion," *MISES User's Guide*, Massachusetts Inst. of Technology Computational Aerospace Sciences Lab., MIT Press, Boston, MA, 1995.

[16]Emery, J. C., Herrig, L. J., Erwin, J. R., and Felix, A. R., "Systematic Two-Dimensional Cascade Test of NACA 65-Series Compressor Blades at Low Speeds," NACA Rept. 1368, 1957.

[17]Denton, J. D., "Loss Mechanisms in Turbomachines," *Journal of Turbomachinery*, Vol. 115, No. 4, Oct. 1993, pp. 621–656.